



**HAL**  
open science

# Decreasing Phanerozoic extinction intensity as a consequence of Earth surface oxygenation and metazoan ecophysiology

Richard Stockey, Alexandre Pohl, Andy Ridgwell, Seth Finnegan, Erik Sperling

► **To cite this version:**

Richard Stockey, Alexandre Pohl, Andy Ridgwell, Seth Finnegan, Erik Sperling. Decreasing Phanerozoic extinction intensity as a consequence of Earth surface oxygenation and metazoan ecophysiology. Proceedings of the National Academy of Sciences of the United States of America, 2021, 118 (41), pp.e2101900118. 10.1073/pnas.2101900118 . hal-03364856

**HAL Id: hal-03364856**

**<https://hal.science/hal-03364856>**

Submitted on 6 Oct 2021

**HAL** is a multi-disciplinary open access archive for the deposit and dissemination of scientific research documents, whether they are published or not. The documents may come from teaching and research institutions in France or abroad, or from public or private research centers.

L'archive ouverte pluridisciplinaire **HAL**, est destinée au dépôt et à la diffusion de documents scientifiques de niveau recherche, publiés ou non, émanant des établissements d'enseignement et de recherche français ou étrangers, des laboratoires publics ou privés.



Distributed under a Creative Commons Attribution 4.0 International License



## **Main Manuscript for**

### **Decreasing Phanerozoic extinction intensity as a consequence of Earth surface oxygenation and metazoan ecophysiology**

Richard G. Stockey<sup>1\*</sup>, Alexandre Pohl<sup>2,3</sup>, Andy Ridgwell<sup>2</sup>, Seth Finnegan<sup>4</sup>, and Erik A. Sperling<sup>1</sup>

<sup>1</sup>Department of Geological Sciences, Stanford University, Stanford, CA, USA

<sup>2</sup>Department of Earth and Planetary Sciences, University of California, Riverside, CA, USA

<sup>3</sup>Biogéosciences, UMR 6282, UBFC/CNRS, Université Bourgogne Franche-Comté, 6 boulevard Gabriel, F-21000 Dijon, France

<sup>4</sup>Department of Integrative Biology, University of California, Berkeley, Berkeley, CA, USA

\*To whom correspondence should be addressed.

**Email:** Richard Stockey (rstockey@stanford.edu)

**Author Contributions:** R.G.S. and E.A.S. designed the research; R.G.S. conducted Earth system modeling with input from A.R.; A.P. and A.R. generated the Ordovician model configuration; R.G.S. conducted ecophysiological modeling; R.G.S. and S.F. conducted quantitative paleobiological analyses; R.G.S. wrote the paper with contributions from all authors.

**Classification:** Physical Sciences/Earth, Atmospheric, and Planetary Sciences

**Keywords:** Extinction, oxygen, ecophysiology, temperature-dependent hypoxia, Earth system evolution

#### **This PDF file includes:**

Main Text  
Figure Captions

1 **Abstract**

2 The decline in background extinction rates of marine animals through geologic time is an  
3 established but unexplained feature of the Phanerozoic fossil record. There is also  
4 growing consensus that the ocean and atmosphere did not become oxygenated to near-  
5 modern levels until the mid-Paleozoic, coinciding with the onset of generally lower  
6 extinction rates. Physiological theory provides us with a possible causal link between  
7 these two observations – predicting that the synergistic impacts of oxygen and  
8 temperature on aerobic respiration would have made marine animals more vulnerable to  
9 ocean warming events during periods of limited surface oxygenation. Here, we evaluate  
10 the hypothesis that changes in surface oxygenation exerted a first-order control on  
11 extinction rates through the Phanerozoic using a combined Earth system and  
12 ecophysiological modeling approach. We find that although continental configuration, the  
13 efficiency of the biological carbon pump in the ocean, and initial climate state all impact  
14 the magnitude of modeled biodiversity loss across simulated warming events,  
15 atmospheric oxygen is the dominant predictor of extinction vulnerability, with metabolic  
16 habitat viability and global ecophysiotype extinction exhibiting inflection points around  
17 40% of present atmospheric oxygen. Given this is the broad upper limit for estimates of  
18 early Paleozoic oxygen levels, our results are consistent with the relative frequency of  
19 high-magnitude extinction events (particularly those not included in the canonical Big  
20 Five mass extinctions) early in the Phanerozoic being a direct consequence of limited  
21 early Paleozoic oxygenation and temperature-dependent hypoxia responses.

22

23 **Significance Statement**

24 The decline in extinction rates through geologic time is a well-established but enigmatic  
25 feature of the marine animal fossil record. We hypothesize that this trend is driven largely  
26 by secular changes in the oxygenation of the atmosphere and oceans, as physiological  
27 principles predict that marine animals would have been more vulnerable to ocean  
28 warming during intervals of geological time with limited atmospheric oxygenation. We

29 test this at a global oceanographic scale by combining models of ocean biogeochemistry  
30 and animal physiology. We show that atmospheric oxygen exerts a first-order control on  
31 the simulated extinction vulnerability of marine animals, highlighting its likely  
32 importance in controlling extinction trends through geologic time.

33

## 34 **Introduction**

35 One of the most striking and poorly understood features of the marine fossil record is a  
36 long-term decline in apparent extinction rates through the Phanerozoic (1–7). First  
37 revealed by analyses of stratigraphic range compilations ~40 years ago (1), this decline  
38 has been a persistent feature in subsequent analyses using expanded databases (8) and  
39 improved extinction rate and richness metrics since then (e.g. (2–7); Figs. 1, S1).  
40 Declining genus-level extinction rates are a consistent feature of Phanerozoic analyses  
41 using a broad range of different richness and extinction rate metrics ((7); Fig. S2, Table  
42 S1), and are not substantially altered by varying temporal binning or controlling for  
43 species/genus ratio (Figs. S1-2, Table S1; *Materials and Methods*). In particular, the  
44 Cambrian and Ordovician Periods stand out as intervals of especially high faunal  
45 turnover ((6, 7, 9); Figs. S1-2), to the point that the early Paleozoic is often treated  
46 separately from the rest of the Phanerozoic in quantitative analyses of extinction (e.g. (7,  
47 10, 11)). Changes in the distribution of lineage ages and geographic range sizes, area of  
48 continental shelf environments, intensity of species interactions, frequency of geological  
49 triggers, stabilization of Earth’s climate, and rock-area sampling biases have all been  
50 proposed as drivers of this trend (10–14). However, despite the long history of study and  
51 numerous proposed explanations, no consensus has been reached regarding the drivers of  
52 much higher early Paleozoic extinction rates vs. those of the later Paleozoic, Mesozoic  
53 and Cenozoic.

54       Secular trends in the oxygenation of the ocean and atmosphere are an  
55 underexplored factor that may help explain changing extinction intensity through time. A  
56 growing body of geochemical proxy evidence suggests that Earth’s surface did not  
57 become oxygenated to near-modern levels until the early-mid Paleozoic (Fig. 1) (15–20)

58 and the most recent generation of long-term carbon cycle models support only limited  
59 early Paleozoic oxygenation (21–23). While early Paleozoic marine oxygen  
60 concentrations were self-evidently above minimum thresholds for aerobic metazoan  
61 metabolism (at least, in the shallow ocean), modern observations clearly show that  
62 variations in dissolved oxygen exert a strong control on marine biodiversity (24–26).  
63 Moreover, experimental respirometry, metabolic theory, and ecophysiological modeling  
64 have demonstrated that the synergistic effects of oxygen and temperature on capacity for  
65 aerobic respiration significantly influence the metabolic viability of marine habitat (27–  
66 32). Following the principle of oxygen and capacity limited thermal tolerance (OCLTT –  
67 see Pörtner (28) for review), the critical partial pressure of oxygen ( $pO_2$ ) required to  
68 sustain resting metabolism increases exponentially with temperature, and the increase in  
69 oxygen supply required for ecologically sustainable populations results in a further  
70 steepening of this exponential relationship (Fig. 2; (33)). Meta-analyses investigating the  
71 sensitivity of modern marine ectotherms to climate-related stressors and the vulnerability  
72 of their fossil representatives to extinction further suggest that physiological traits of  
73 modern marine animals can be generally scaled to extinction sensitivity to ancient climate  
74 perturbations (34).

75         Seawater  $pO_2$  would have been dramatically lower in an early Paleozoic Earth  
76 system with limited surface oxygenation, leading to the prediction that marine ectotherms  
77 would have been substantially more vulnerable to temperature-dependent hypoxia, and  
78 therefore climate-driven extinction, due to reduced thermal safety margins in poorly  
79 oxygenated ancient oceans (Fig. 2; (35)). This logic further leads to the implication that  
80 dissolved oxygen was likely important to the structure of marine ecosystems at  
81 concentrations well above critical hypoxic thresholds that have previously been invoked  
82 for the evolution of early animals (36, 37), as is observed at regional scales in modern  
83 marine environments (29–31, 38). Recent advances in Earth system modeling provide an  
84 opportunity to test this hypothesis at the planetary-scale and to explicitly distinguish the  
85 role of changes in surface oxygenation through the Phanerozoic from variations in  
86 continental configuration, biological carbon cycling and climate state.

87           Our approach is two-fold – incorporating both Earth system and ecophysiological  
88 modeling. First, using an Earth system model of intermediate complexity (cGENIE (39) –  
89 see *Materials and Methods* and *Supplementary Information*) and an ensemble  
90 experimental approach, we generate a suite of three-dimensional realizations of potential  
91 marine environmental conditions. These Earth system model experiments span a range of  
92 scenarios for atmospheric O<sub>2</sub> and CO<sub>2</sub> concentrations (Fig. 3a) in order to address  
93 uncertainty associated with reconstructions of these variables through geologic time (e.g.  
94 Fig 1b). Atmospheric CO<sub>2</sub> concentrations are varied to force global climate in our  
95 experiments and solar forcing is kept constant for each ensemble (Fig. 3). Simulating the  
96 potential three-dimensional structure of past oceans in these experiments is critical: in the  
97 upper ocean, oxygen and temperature both decrease with depth, but have opposite  
98 gradients with respect to latitude (33, 38). Temperature gradients decrease towards the  
99 poles, while subsurface oxygen gradients increase. Because aerobic habitability for  
100 marine animals involves the synergistic combination of oxygen and temperature (29, 34,  
101 35, 38), elucidating the spatial complexity of the environmental landscape of ancient  
102 oceans is required to appropriately understand biological responses to environmental  
103 perturbations.

104           We additionally identify key boundary conditions that have significantly changed  
105 through Earth history and may offer alternative explanations for the trends in extinction  
106 rates observed in the fossil record. 1) Continental configuration, which affects latitudinal  
107 habitat (i.e. continental shelf) distribution, as well as ocean circulation (and resulting  
108 temperature and oxygen gradients), and could therefore have modulated the susceptibility  
109 of animals to extinction (33, 40, 41). 2) The efficiency of the biological carbon pump in  
110 the ocean, which exerts a control on the distribution of oxygen in the upper water column  
111 (42) and has been previously identified as important in differentiating earlier Paleozoic  
112 vs. Mesozoic-Cenozoic ocean redox conditions (17). 3) Climate state, which directly  
113 impacts ocean surface temperatures (and by extension dissolved marine oxygen) and  
114 therefore influences how close animals at a given latitude are living to their physiological  
115 limits (29, 38).

116 Utilizing model ocean temperatures and dissolved oxygen concentrations from  
117 this suite of 3D realizations, we then employ the recently developed Metabolic Index (29,  
118 33, 38) in order to evaluate the proportion of modern marine ectotherms (based upon  
119 available experimental respirometry data) that could survive in these simulated  
120 environments. While we do not attempt to directly simulate taxonomic diversity, the  
121 Metabolic Index provides us with a means to mechanistically assess the physiological  
122 ecotypes (herein, ecophysiotypes) that can contribute to biodiversity. We apply a  
123 probabilistic representation of temperature-dependent hypoxia responses (Fig. 2) to  
124 define ‘metabolic habitat viability’, a global metric describing the percentage of feasible  
125 ecophysiotypes that can live anywhere in the shelf environments of our 3D ocean models.  
126 Following other paleoecological modeling approaches (e.g. (41)), we focus our analyses  
127 on shelf environments because they constitute the majority of the Phanerozoic fossil  
128 record and host the majority of marine biodiversity in the modern, although we provide  
129 complimentary simulations for the entire global ocean.

130 Finally, we estimate global extinction sensitivity across a range of atmospheric O<sub>2</sub>  
131 concentrations to link our ecophysiological models more directly to the trends we observe  
132 in the geologic record. We model ‘global ecophysiotype extinction’ as the predicted loss  
133 of ecophysiotypes across a nominal warming event of ~5°C (as defined by mean  
134 temperature change in the equatorial surface ocean; Fig. S3, Table S2). These warming  
135 events are represented by Earth system models separated by two doublings of  
136 atmospheric CO<sub>2</sub>, and are designed to mimic relatively extreme (but not infrequent)  
137 examples of climate variability known to have occurred throughout Earth history (43,  
138 44). We performed this extinction sensitivity estimate for all scenarios of atmospheric O<sub>2</sub>  
139 and for each ensemble (continental configuration, biological pump efficiency; Figs. 3,  
140 S3) across multiple baseline climate states. We further explore the consistency of our  
141 results across different thresholds for minimum habitat area (number of equal area ocean  
142 model cells) and tolerances for proportional habitat loss, as well as across deviations from  
143 the distributions of physiological tolerances observed in modern marine ectotherms.  
144 Thus, by combining ecophysiology and ensemble Earth system modeling, we evaluate the  
145 vulnerability of marine ectotherms to warming events at a range of atmospheric O<sub>2</sub> levels

146 in a framework that is neutral to the selective advantage of different ecophysiotypes and  
147 explores the relative impacts of other aspects of Phanerozoic Earth system evolution on  
148 marine animal ecophysiology.

149

## 150 **Results**

### 151 *Metabolic habitat viability*

152 Metabolic habitat viability – the total number of ecophysiotypes that can live in  
153 the shelf environments of each ancient ocean realization – is shown in Figure 4 for our  
154 ensemble of simulations employing an Ordovician continental configuration and Figure  
155 S4 for all other Earth system model ensembles. In all ensembles, metabolic habitat  
156 viability exhibits a positive relationship with atmospheric O<sub>2</sub> and a negative relationship  
157 with global temperature, resulting in a sigmoidal relationship between atmospheric O<sub>2</sub>  
158 and metabolic habitat viability for a given climate state. While our primary analyses  
159 focus on shelf environments, very similar trends are observed when the entire ocean is  
160 considered as potential habitat for marine animals (Figs. S5-6). Using entire 3D ocean  
161 models often results in slightly higher estimates of metabolic habitat viability because  
162 cooler and (at higher atmospheric O<sub>2</sub> levels) well-oxygenated deep ocean environments  
163 may act as refugia, despite being unlikely diversity hotspots for other reasons such as  
164 food supply (45, 46). The latitudinal distribution of viable ecophysiotypes is similar  
165 between continental configurations (Figs. 3, S3), with more ecophysiotypes generally  
166 able to inhabit cooler polar regions of the surface ocean. Identifying oceanographic and  
167 tectonic drivers of regional differences in viable ecophysiotype biogeography between  
168 continental configurations is an interesting avenue for future research, but this would  
169 require tuning model ensembles to precisely equivalent climate states and is therefore  
170 beyond the scope of this study.

171 Changes in metabolic habitat viability between cooler and warmer climate states  
172 allow us to begin linking ecophysiology to extinction sensitivity under different scenarios  
173 of atmospheric oxygenation (Fig. 4). The percentage change in metabolic habitat viability

174 between colder and warmer ocean simulations increases as atmospheric oxygen decreases  
175 from modern levels (100% preindustrial atmospheric levels, PAL), reaching maximum  
176 values at atmospheric O<sub>2</sub> concentrations reconstructed for the early Paleozoic (<40-50%  
177 PAL – grey envelope in Figs. 4, S4). Furthermore, because extinction is expected to track  
178 the proportional rather than absolute loss of ecophysiotypes (33, 40), differences in  
179 metabolic habitat viability would therefore be amplified to result in high levels of  
180 warming-driven extinction at lower levels of atmospheric oxygenation reconstructed for  
181 the early Paleozoic (e.g. 20% PAL). In such cases, the number of viable ecophysiotypes  
182 in any low-O<sub>2</sub> scenario is much lower, leading to greater proportional change despite a  
183 similar absolute change in metabolic habitat viability to that predicted at higher O<sub>2</sub> levels  
184 (e.g. 80% PAL). Our analyses thus demonstrate that the expected proportional loss of  
185 ecophysiotypes during a global warming event would be substantially higher under the  
186 limited surface oxygenation scenarios hypothesized for the early Paleozoic than for  
187 modern (or, more broadly, post-mid-Paleozoic) levels of oxygenation.

188

### 189 *Sensitivity of global extinction simulations*

190         When we simulate the impacts of warming events on the extinction of marine  
191 animals, the general trend of greater predicted extinction at lower atmospheric oxygen  
192 levels is a common feature of all ensemble experiments (Figs. 5, S7-12). There is  
193 variation in the absolute magnitude of simulated global ecophysiotype extinction between  
194 the different continental configurations tested in our ensembles. However, we do not  
195 observe any time-dependent trends in extinction sensitivity between progressive  
196 continental reconstructions and the most striking feature of the results remains the non-  
197 linear increase in global ecophysiotype extinction with declining oxygenation (Figs. 5,  
198 S7-12). Below 10% PAL O<sub>2</sub>, the relationship between modeled extinction and  
199 atmospheric oxygen is less predictable. However, the initial pool of viable pre-extinction  
200 ecophysiotypes in these simulations is very small at low O<sub>2</sub> levels (Figs. 3, 4, S4-6),  
201 suggesting that this inconsistency may partially be a product of sample size (as supported  
202 by wider envelopes in Figures 5, S7-8, S11) and the limited experimental respirometry

203 data for animals that live in low-oxygen environments (47). We find that modeled  
204 extinction is high at low atmospheric oxygen levels for the Ordovician configuration  
205 regardless of the efficiency of the biological pump (Fig. S7), suggesting that despite its  
206 role in controlling the distribution of oxygen in the upper water column this factor is of  
207 secondary importance compared to atmospheric O<sub>2</sub>. A shallower remineralization depth  
208 does slightly reduce simulated extinction sensitivity at low atmospheric O<sub>2</sub> (~5-20%  
209 PAL), although the same caveat of small initial ecophysiotype population size applies.

210         Increasing the baseline temperature in our extinction simulations (i.e. testing for  
211 any initial climate state dependence of extinction susceptibility), results in increased  
212 predicted global ecophysiotype extinction for all three continental configurations (Fig.  
213 S8). A corresponding decrease in modeled ecophysiotype extinction is generally observed  
214 at cooler baseline temperatures. Cool, low O<sub>2</sub> (<20% PAL) Ordovician simulations are a  
215 minor exception to this general rule, suggesting that continental configuration may exert a  
216 second-order control on the climate state dependence of extinction vulnerability. The  
217 impact of initial climate state on simulated ecophysiotype extinction appears less  
218 dramatic than the impact of atmospheric oxygen, particularly in light of the apparent  
219 inflection in modeled extinction observed around upper estimates for early Paleozoic O<sub>2</sub>  
220 levels. However, we note that pre-extinction climate state impacts modeled  
221 ecophysiotype extinction more than any other Earth system boundary condition explored  
222 in this study.

223         Altering the assumptions of our ecophysiological modeling approach does not  
224 dramatically impact the observed relationship between predicted extinction and  
225 atmospheric oxygen. In our primary analyses, we define ecophysiotype extinction as only  
226 occurring when no cells in our simulated shelf environments are viable for an  
227 ecophysiotype, or (equivalently) when 100% of metabolically viable habitat area is lost.  
228 Increasing the minimum number of inhabited ocean cells required to survive a warming  
229 event or decreasing the proportional habitat loss required for extinction moderately  
230 increases modeled global ecophysiotype extinction (Figs. S9-10). The differences in the  
231 shape of these responses highlight the importance of these parameters and the second-

232 order effects of continental configuration. However, the overall trend of decreasing  
233 extinction intensity with increased atmospheric O<sub>2</sub>, with an apparent inflection point  
234 generally around 40% PAL, is consistent across all of these simulations. Similar trends  
235 are observed when investigating the impacts of varying the distributions used to  
236 parameterize physiological responses ( $A_o$  – the inverse of the hypoxic threshold; and  $E_o$  –  
237 the temperature-dependency of the hypoxic threshold). While varying the distributions of  
238  $A_o$  and  $E_o$  does impact the magnitude of simulated global ecophysiotype extinction and  
239 the steepness of the inflection around 40% PAL O<sub>2</sub> (Fig. S11), the overarching trends of  
240 increasing predicted extinction with decreasing atmospheric oxygen (down to at least  
241 20% PAL O<sub>2</sub>) are not impacted. The size of the synthetic population of ecophysiotypes  
242 (*Materials and Methods*) has no noticeable effect on the analyses illustrated in Figure 5  
243 (Fig. S12).

244

## 245 **Discussion**

246 Using a coupled Earth system and ecophysiological modeling approach, our analyses  
247 suggest that oxygenation of the shallow ocean (as modulated by atmospheric oxygen  
248 levels) is the dominant factor in governing the vulnerability of marine animals to  
249 extinction during warming events. These results remain consistent when complex  
250 oceanographic relationships between temperature and seawater oxygenation and  
251 uncertainties in ocean circulation, biological pump efficiency, climate state, and habitat  
252 area thresholds are taken into account. Critically, the relationship we observe between  
253 simulated global ecophysiotype extinction and atmospheric oxygen is non-linear, with an  
254 apparent inflection point around 40% PAL O<sub>2</sub> (Fig. 5). This broadly coincides with the  
255 upper limit of estimates for early Paleozoic atmospheric oxygen (Fig. 1; (15, 17)),  
256 supporting the hypothesis that relatively low atmospheric oxygen levels created boundary  
257 conditions under which high-magnitude extinction events were more likely to occur as a  
258 product of climate variability.

259 While atmospheric oxygen is the primary control on extinction sensitivity in our  
260 simulations, our analyses show that other factors modulate the response to varying  
261 degrees. This is unsurprising considering how these factors affect the three-dimensional  
262 oxygen-temperature landscape of the ocean. In particular, our analyses indicate that  
263 continental configuration may play an important secondary role in governing  
264 ecophysiotype extinction vulnerability at the global scale (Fig. 5), although this is  
265 difficult to clearly separate from minor climatic differences between ensembles. Notably,  
266 we do not observe time-correlative trends between the three continental configurations  
267 that could help explain the secular extinction rate observations from the fossil record. In  
268 other words, we do not find that extinction sensitivity in the polar-biased and relatively  
269 compact continental configuration of the Ordovician is particularly different from that of  
270 the more evenly latitudinally distributed and dispersed configuration of the Paleocene  
271 when compared to the differences associated with changing atmospheric O<sub>2</sub>. The  
272 efficiency of the biological pump (simulated here as a difference in prescribed  
273 remineralization depths in the ocean) is also thought to have changed through the  
274 Phanerozoic (17). However, we find that the differences in simulated extinction  
275 sensitivity are minimal and (if anything) in opposition to the influence of changes in  
276 atmospheric oxygenation (Fig. S7). This is likely because both continental configuration  
277 and carbon remineralization depth mainly change oxygen distributions in the deeper  
278 ocean, whereas most animals are living (and dying) in the surface ocean, which is closely  
279 coupled to the O<sub>2</sub> concentration of the atmosphere. Finally, while the habitat area  
280 thresholds we used to define simulated extinction and specific parameterization of  
281 physiological traits do impact the slope and magnitude of the observed relationship  
282 between atmospheric oxygen and extinction (in expected directions; Figs. S9-11), the first  
283 order trends remain consistent regardless of how we parametrize our ecophysiological  
284 extinction model.

285 We additionally find that an important climate state-dependence exists for  
286 ecophysiological extinction sensitivity. Marine animals are expected to be living closer to  
287 their thermal limits as defined by oxygen and capacity limited thermal tolerance in  
288 warmer environments based on observations from modern tropical marine habitats (Fig.

289 2; (29, 38)), with implications for broader areas of the ocean in ancient greenhouse  
290 climates. We provide further model support for this hypothesis by demonstrating  
291 increased simulated extinction magnitudes in warmer climate states (Fig. S8). Very warm  
292 early Paleozoic sea surface temperatures have been reconstructed using geochemical  
293 paleothermometry (48–50), suggesting that this phenomenon could also provide some  
294 explanatory power for the frequency of high magnitude extinctions. However, while  
295 recent advances in paleothermometry have shown considerable potential in constraining  
296 Ordovician climate dynamics (50), there is still currently limited consensus on directional  
297 trends in early Phanerozoic sea surface temperatures, especially in the earliest Paleozoic  
298 (51–53). In contrast, reconstructions of atmospheric oxygen are increasingly consistent,  
299 even if the absolute concentrations are poorly constrained (Fig. 1). This discussion should  
300 not be framed as a question of oxygen *versus* temperature; inherent to the concept of  
301 temperature-dependent hypoxia is that both interact to determine aerobic safety margins  
302 (Fig. 2; (29, 34, 38)). We therefore suggest that atmospheric oxygen can confidently be  
303 established as a first-order control on early Phanerozoic extinction rates, and that  
304 potentially high sea surface temperatures through the same time interval may have  
305 amplified the effect of limited surface oxygenation. Changes in the latitudinal focus of  
306 fossil sampling through the Phanerozoic may also bias extinction rate estimates slightly  
307 towards environments with warmer baseline temperatures in the early Paleozoic when  
308 well-sampled paleocontinents were mainly situated at low latitudes (54). However, the  
309 lack of similarly high long-term extinction rates across other intervals with low-latitude  
310 sampling biases indicates that this cannot fully explain the trends we seek to explain here  
311 and that atmospheric oxygen (potentially compounded by warm global climate) is a more  
312 probable first-order driver.

313         The plausibility of temperature-dependent hypoxia as a driver of high early  
314 Paleozoic extinction rates is supported by links between sea-level changes, ocean  
315 deoxygenation and extinctions during this interval of geologic time. The Cambrian-  
316 Ordovician biomere-style extinction events are a major component of the  
317 characteristically high early Paleozoic extinction rates (9). These events, predominantly  
318 observed in the trilobite fossil record (e.g. (55)), have long been recognized as associated

319 with sedimentological evidence of sea-level change, possible thermocline migration and  
320 ocean anoxia (56, 57). Stable isotope geochemistry provides further evidence that the  
321 biomere events were linked to major marine carbon and sulfur cycle perturbations,  
322 consistent with ocean warming and deoxygenation (58–61). Similar inferences of ocean  
323 anoxia and rapid sea-level change have been made for the early-middle Cambrian  
324 Botomian extinction event (62). In contrast, multiple Mesozoic and Cenozoic  
325 hyperthermals (including the Paleocene-Eocene Thermal Maximum and Cretaceous  
326 Oceanic Anoxic Event 2) that exhibit similar broad patterns of environmental change (43,  
327 63–65) do not correlate with global marine extinctions of comparably high magnitude  
328 (Fig. 1; (9)). Our analyses demonstrate that the effects of changing atmospheric  
329 oxygenation on the thermal safety margins of marine ectotherms (Fig. 2) may account for  
330 this discrepancy in extinction magnitude between events with similar signatures of  
331 environmental change. Our simulations of metabolic habitat viability also offer a  
332 potential mechanism for the high origination rates observed through the early Paleozoic  
333 (6, 7) – particularly if simple logistic models of extinction and subsequent recovery (i.e.  
334 origination; e.g. (4, 66)) can be broadly applied to the Phanerozoic fossil record.  
335 However, we focus upon warming driven extinction events because fewer assumptions  
336 regarding the evolutionary advantages of different ecophysiotypes (and how they relate to  
337 the rate at which physiological diversity increases in cool climate states) are required for  
338 these models, which simply simulate the instantaneous loss of viable ecophysiotypes.

339 Our combined Earth system and ecophysiological modeling approach provides a  
340 methodological advance in moving from simple correlation to more mechanistic  
341 understanding of how environmental change impacted marine ecosystems through Earth  
342 history. The use of physiology as a conceptual bridge between the fossil and geochemical  
343 records is of clear appeal for establishing a mechanistic understanding of animal-  
344 environment interactions from the geologic record (67). However, the power of Earth  
345 system models in simulating the ecophysiological responses of marine animals to deep-  
346 time environmental change is only recently being explored (e.g. (33, 41)). We apply  
347 simple assumptions about the diversification of ecophysiotypes (i.e. that ecophysiotypes  
348 proliferate in times of stability and become inviable during warming events) to test the

349 hypothesis that limited atmospheric oxygenation would increase physiological  
350 vulnerability to ocean warming events on geologic timescales. For increasingly accurate  
351 models of animal-environment interactions through the Phanerozoic (for example, ones  
352 that directly simulate latitudinal gradients in taxonomic diversity), other key variables  
353 involved in these interactions will need to be incorporated. At the organism-scale,  
354 physiological traits including vulnerability to ocean acidification, food supply limitation  
355 and possible variations in physiological responses are all likely important variables. For  
356 example, the different buffering capacities of marine animal groups have previously been  
357 invoked to explain differential extinction selectivity (68, 69). Meta-analytical approaches  
358 also suggest that sensitivity to climate related stressors correlates with genus survival  
359 across ancient extinction events in higher-level taxonomic groups (34), further indicating  
360 that differences in physiological tolerances between marine clades may be an important  
361 consideration when applying ecophysiological principles to Earth history. While we  
362 demonstrate that our results are consistent across a range of deviations from mean  
363 modern physiological responses, it will hopefully become feasible to begin linking  
364 physiological traits more directly to extinct animal groups based on phylogenetic and  
365 adaptive principles as the availability of experimental respirometry data characterizing  
366 temperature-dependent hypoxic responses of marine ectotherms increases. At the  
367 macroecological scale, migration (as applied in Saupe et al. (41)), species interactions,  
368 and resource competition also play key roles in governing population and species  
369 responses to environmental change. As model frameworks for deep-time animal-  
370 environment interactions develop in terms of both ecophysiological and biogeochemical  
371 realism, the temporal-spatial resolution of paleontological and geochemical databases  
372 will also be critical to the explanatory power of these methodologies, as will techniques  
373 addressing the limitations and biases inherent to the geologic record (4–6, 13, 54, 70–72).

374

## 375 **Conclusions**

376 Using a novel ensemble Earth system and ecophysiological modeling framework, we  
377 demonstrate that atmospheric oxygen levels likely exerted a first-order control on

378 extinction vulnerability through the Phanerozoic. Our model analyses illustrate that the  
379 theoretical predictions of oxygen and capacity limited thermal tolerance are expected to  
380 have globally significant implications, resulting in dramatically increased extinction of  
381 marine animals under varying climatic conditions during geological periods with limited  
382 surface oxygenation. While warmer initial climate states increase the magnitude of our  
383 simulated extinctions, and continental configuration and the strength of the biological  
384 pump also have minor impacts on our predictions, the trend of increased extinction  
385 vulnerability with early Paleozoic levels of atmospheric oxygen is dominant across all of  
386 our simulations. We therefore argue that the exceptional frequency of high-magnitude  
387 extinction events in the early Paleozoic was primarily a consequence of limited surface  
388 oxygenation and temperature-dependent hypoxia responses in marine animals.

389

## 390 **Materials and Methods**

### 391 *Quantitative paleobiology*

392 We performed a series of quantitative paleobiological analyses to evaluate evidence for  
393 declining extinction rates through the Phanerozoic. We adapted methods from Kocsis et  
394 al. (7) to generate new reconstructions and statistical analyses of extinction rates through  
395 the Phanerozoic specifically for marine ectotherms, using an updated download from the  
396 Paleobiology Database (PBDB) and omitting endothermic and/or exclusively air-  
397 breathing higher-level marine taxa (marine mammals, marine reptiles and turtles). We  
398 generated reconstructed extinction rates using three richness metrics (classical  
399 rarefaction, raw occurrences and shareholder quorum subsampling) and four extinction  
400 rate metrics (second-for-third substitution, corrected three-timer, gap-filler and per-  
401 capita). We applied these metrics to generate reconstructions for all genera both at stage  
402 resolution and using the PBDB ~10 million year bins. To investigate the potential impact  
403 of changing species to genus ratios through the Phanerozoic (e.g. (73)), we further  
404 conducted the same analyses on filtered datasets, generating reconstructions all genera,  
405 genera with a single accepted named species, genera with 2 species, genera with 3

406 species, and genera with 4 or more accepted named species (Fig. S1). For shareholder  
407 quorum subsampling analyses we used a quorum level of 0.5 to accommodate lower  
408 sampling intensity in filtered datasets (as supported by Boag et al. (32)) and remain  
409 within the >0.4 quorum range suggested by previous authors (7). Figure 1 is a summary  
410 of the top-right panel of Figure S1, including all genera at stage resolution. We further fit  
411 cross-validated LOESS models to our reconstructed extinction rates to evaluate whether  
412 early Paleozoic decreases in extinction rates were a major feature of the full Phanerozoic  
413 record (Fig. S2). Finally, we generated Spearman's correlation coefficients to investigate  
414 the statistical significance of temporal declines in extinction rates across all of our  
415 treatments (Table S1). Adapted code from Kocsis et al. (7) and filtered Paleobiology  
416 Database download are available at [https://github.com/richardstockey/cGENIE-](https://github.com/richardstockey/cGENIE-metabolic_index_extinction)  
417 [metabolic\\_index\\_extinction](https://github.com/richardstockey/cGENIE-metabolic_index_extinction) and are assigned a DOI: 10.5281/zenodo.5143583

418

#### 419 *Earth system modeling*

420 cGENIE is an Earth system model of intermediate complexity, designed for the spatially-  
421 explicit biogeochemical characterization of global-scale paleoceanographic problems  
422 (39). We create a range of 3D realizations of ocean environmental conditions by running  
423 ensembles of model experiments. The experiments in each ensemble are run for 10,000 or  
424 20,000 years (depending on the time required for dissolved marine O<sub>2</sub> and seawater  
425 temperature to reach steady state), with a range of assumptions regarding atmospheric  
426 pCO<sub>2</sub> specific to each continental configuration based upon changing solar luminosity  
427 and albedo (Fig. 3), and a range of atmospheric pO<sub>2</sub> scenarios based upon the range of  
428 estimates from geochemical proxy data and biogeochemical box modeling (Fig. 1). We  
429 apply this ensemble treatment to three ancient continental configurations, chosen for their  
430 relatively even temporal spread across the Phanerozoic and history of use in previous  
431 paleoclimate studies – a Paleocene configuration (~55 Ma) (43), a Permian configuration  
432 (~251 Ma) (74), and an Ordovician configuration (~450 Ma) (based on the 8 PAL CO<sub>2</sub>  
433 FOAM simulation of Pohl et al. (75) – see *Supplementary Information*). For each of these  
434 ancient configurations, we apply age-appropriate solar luminosity (76). Finally, in the

435 Ordovician continental configuration, we explore the possible influence of postulated  
436 Phanerozoic changes in organic matter remineralization depth in the ocean (17, 42) –  
437 testing ~1/3 modern, or specifically 200m, e-folding depth (42).

438 We extract the mean annual ocean temperature and ocean oxygen concentration  
439 during the last simulated year for each ocean grid cell and generate corresponding  
440 seawater oxygen partial pressure ( $pO_2$ ) values (following the methods of Hofmann et al.  
441 (77)). Changing solar luminosity and continental configuration results in different mean  
442 sea surface temperatures for the same atmospheric  $CO_2$  assumption. We therefore  
443 identify the  $pCO_2$  values for each continental configuration that create comparable  
444 climate simulations (Table S2 and *Supplementary Information*). These climate scenarios  
445 are compared using the mean equatorial ( $3.2^\circ S$  to  $3.2^\circ N$ , 0-80m depth) surface ocean  
446 temperature for each model (Figs. 4, S4-6, Table S2).

447 The code for the version of the ‘muffin’ release of the cGENIE Earth system  
448 model used in this paper is tagged as v0.9.19 and is assigned a DOI:  
449 10.5281/zenodo.4473048. Configuration files for the specific experiments presented in  
450 the paper can be found in the directory: genie-userconfigs/MS/stockeyetal.PNAS.2021.  
451 Details on the experiments, plus the command line needed to run each one, are given in  
452 the readme.txt file in that directory. All other configuration files and boundary conditions  
453 are provided as part of the code release.

454 A manual detailing code installation, basic model configuration, tutorials covering  
455 various aspects of model configuration and experimental design, plus results output and  
456 processing, is assigned a DOI: 10.5281/zenodo.4469678.

457

#### 458 *Ecophysiological simulations of animal-environment interactions*

459 We combine our ensemble Earth system modeling experiments with a probabilistic  
460 ecophysiological model of extinction vulnerability. The Metabolic Index, as defined by  
461 Deutsch et al. (29) and Penn et al. (33), is configured here to calculate the proportion of

462 modern marine ectotherms (based on described temperature-dependent hypoxia  
 463 responses) that can inhabit each ocean cell in the cGENIE Earth system model.

$$464 \quad \text{Metabolic habitat viability} = \sum_{\min(A_o, E_o, \phi_{\text{crit}})}^{\max(A_o, E_o, \phi_{\text{crit}})} A_o \frac{pO_2}{\exp\left[\frac{-E_o}{k_B} \left(\frac{1}{T} - \frac{1}{T_{\text{ref}}}\right)\right]} > \phi_{\text{crit}}$$

465 (Eqn. 1)

466 At the individual organism scale,  $A_o$  is the inverse of the hypoxic threshold of the  
 467 organism (the minimum required seawater  $pO_2$  ( $P_{\text{crit}}$ ) to sustain resting aerobic  
 468 metabolism),  $E_o$  is the temperature-dependency of the hypoxic threshold and  $\phi_{\text{crit}}$  is the  
 469 multiplicative increase in oxygen supply that is required to support ecologically  
 470 sustainable populations (calculated based on biogeographic distribution, relative to  
 471 experimental respirometry measurements of resting metabolism). In our modeling  
 472 approach, these variables are parametrized by probability density functions based on  
 473 observations from laboratory experiments and species distributions (Fig. 2; following  
 474 Penn et al. (33)). Seawater temperature and  $pO_2$  are environmental variables generated  
 475 through the Earth system modeling approach described above (Fig. 3). All other variables  
 476 are constant ( $k_B$  is the Boltzmann constant,  $T_{\text{ref}}$  is a reference temperature of 15°C). In  
 477 our analyses, we simulate 1000 ecophysiotypes, sampled from probability distributions of  
 478  $A_o$ ,  $E_o$  and  $\phi_{\text{crit}}$ , and map which cells (if any) in each cGENIE ocean model are habitable  
 479 for each ecophysiotype (see Figure S12 for exploration of the number of ecotypes used).

480 Metabolic habitat viability, as defined here, quantifies the proportion of these  
 481 modeled ecophysiotypes that can live in the non-polar shelf environments (defined as any  
 482 cell adjacent to continental land mass in the top 3 layers of the cGENIE ocean, or  
 483 <283.8m water depth) of each global ocean model. See Figures S5-6 for sensitivity  
 484 analyses using the entire global ocean model, rather than shelf environments alone. Polar  
 485 environments (>70°N and <70°S) are excluded from all analyses due to the coarse model  
 486 resolution of polar ocean environments (e.g. in a Paleocene northern polar ocean) in  
 487 cGENIE and to reduce local non-linear responses to sea ice extent.

488 We further simulate extinction as the global loss of ecophysiotypes between two  
489 CO<sub>2</sub> scenarios at the same O<sub>2</sub> level. Specifically, we evaluate the proportional loss of  
490 ecophysiotypes between baseline climate states (relatively cool, approximately pre-  
491 industrial mean equatorial surface ocean temperatures – *Supplementary Information*) and  
492 equivalent model scenarios that have undergone ~5°C equatorial warming (Table S2;  
493 modeling a nominal hyperthermal event of roughly the same magnitude as the Paleocene-  
494 Eocene Thermal Maximum (43)) at each atmospheric O<sub>2</sub> level. Global ecophysiotype  
495 extinction is thus defined as the proportion of ecophysiotypes that were viable in shelf  
496 environments of the colder baseline simulation but are no longer viable in any continental  
497 shelf cell of the warmer ocean simulation. Sensitivity analyses exploring the number of  
498 viable cells required to survive a simulated warming event, and the proportional habitat  
499 loss required to drive extinction, are shown in Figures S9-10. Additional sensitivity  
500 analyses exploring deviations from the distributions of  $A_o$  and  $E_o$  defined in Penn et al.  
501 (33) are shown in Figure S11. In these analyses, “low” and “high” distributions have  
502 mean values defined by the 25<sup>th</sup> and 75<sup>th</sup> percentiles of the distributions used in our  
503 primary analyses, and half of the variance of those distributions. In plots of global  
504 ecophysiotype extinction in shelf environments, we summarize the distribution of results  
505 from 100 different simulated populations of 1000 randomly sampled ecophysiotypes to  
506 illustrate the range of sampling-related uncertainty in our probabilistic approach to  
507 ecophysiological modeling. All plots of single ecotype populations (i.e. those with points  
508 rather than envelopes – Figs. 4, S4-6) use the same randomly sampled population.

509 R scripts to reproduce the ecophysiological analyses and associated figures are  
510 available at [https://github.com/richardstockey/cGENIE-metabolic\\_index\\_extinction](https://github.com/richardstockey/cGENIE-metabolic_index_extinction) and  
511 are assigned a DOI: 10.5281/zenodo.5143583

## 512 **Acknowledgements**

513 We thank Thomas Boag and Justin Penn for helpful discussion. R.G.S. and E.A.S.  
514 acknowledge support from National Science Foundation grant EAR1922966. R.G.S.  
515 acknowledges support from the NASA Astrobiology Institute Early Career Collaboration  
516 Award. A.R acknowledges support from the Heising-Simons Foundation. This project

517 has received funding from the European Union's Horizon 2020 research and innovation  
518 programme under the Marie Skłodowska-Curie grant agreement No. 838373. cGENIE  
519 simulations were performed on Earth system modelling cluster facility at University of  
520 California Riverside. Ecophysiological analyses of cGENIE models were performed on  
521 the Sherlock cluster at Stanford University. We thank Stanford University and the  
522 Stanford Research Computing Center for providing computational resources and support  
523 that contributed to this research.

524

525

526

527

- 529 1. D. M. Raup, J. J. Sepkoski, Mass extinctions in the marine fossil record. *Science* **215**, 1501–1503  
530 (1982).
- 531 2. M. Foote, Origination and extinction components of taxonomic diversity: general problems.  
532 *Paleobiology* **26**, 74–102 (2000).
- 533 3. M. Foote, Origination and extinction through the Phanerozoic: A new approach. *J. Geol.* **111**, 125–  
534 148 (2003).
- 535 4. J. Alroy, Dynamics of origination and extinction in the marine fossil record. *Proc. Natl. Acad. Sci.*  
536 *U. S. A.* (2008) <https://doi.org/10.1073/pnas.0802597105>.
- 537 5. J. Alroy, A more precise speciation and extinction rate estimator. *Paleobiology* **41**, 633–639  
538 (2015).
- 539 6. B. Kröger, F. Franeck, C. M. Ø. Rasmussen, The evolutionary dynamics of the early Palaeozoic  
540 marine biodiversity accumulation. *Proc. R. Soc. B Biol. Sci.* **286** (2019).
- 541 7. Á. T. Kocsis, C. J. Reddin, J. Alroy, W. Kiessling, The r package divDyn for quantifying diversity  
542 dynamics using fossil sampling data. *Methods Ecol. Evol.* **10**, 735–743 (2019).
- 543 8. J. Alroy, *et al.*, Effects of sampling standardization on estimates of Phanerozoic marine  
544 diversification. *Proc. Natl. Acad. Sci.* **98**, 6261–6266 (2001).
- 545 9. R. K. Bambach, A. H. Knoll, S. C. Wang, Origination, extinction, and mass depletions of marine  
546 diversity. *Paleobiology* **30**, 522–542 (2004).
- 547 10. S. Finnegan, J. L. Payne, S. C. Wang, The Red Queen revisited: reevaluating the age selectivity of  
548 Phanerozoic marine genus extinctions. *Paleobiology* **34**, 318–341 (2008).
- 549 11. J. L. Payne, S. Finnegan, The effect of geographic range on extinction risk during background and  
550 mass extinction. *Proc. Natl. Acad. Sci. U. S. A.* **104**, 10506–10511 (2007).
- 551 12. S. E. Peters, M. Foote, Determinants of extinction in the fossil record. *Nature* **416**, 420–424 (2002).
- 552 13. S. E. Peters, Environmental determinants of extinction selectivity in the fossil record. *Nature* **454**,  
553 626–629 (2008).
- 554 14. J. L. Payne, A. Bachan, N. A. Heim, P. M. Hull, M. L. Knope, The evolution of complex life and  
555 the stabilization of the Earth system. *Interface Focus* (2020)  
556 <https://doi.org/10.1098/RFS.2019.0106>.
- 557 15. E. A. Sperling, *et al.*, Statistical analysis of iron geochemical data suggests limited late Proterozoic  
558 oxygenation. *Nature* **523**, 451–454 (2015).
- 559 16. T. W. Dahl, *et al.*, Devonian rise in atmospheric oxygen correlated to the radiations of terrestrial  
560 plants and large predatory fish. *Proc. Natl. Acad. Sci. U. S. A.* **107**, 17911–17915 (2010).
- 561 17. W. Lu, *et al.*, Late inception of a resiliently oxygenated upper ocean. *Science* **361**, 174–177 (2018).
- 562 18. M. W. Wallace, *et al.*, Oxygenation history of the Neoproterozoic to early Phanerozoic and the rise  
563 of land plants. *Earth Planet. Sci. Lett.* **466**, 12–19 (2017).
- 564 19. D. A. Stolper, C. B. Keller, A record of deep-ocean dissolved O<sub>2</sub> from the oxidation state of iron in  
565 submarine basalts. *Nature* **553**, 323–327 (2018).
- 566 20. E. A. Sperling, *et al.*, A long-term record of early to mid-Paleozoic marine redox change. *Sci. Adv.*  
567 **7**, eabf4382 (2021).
- 568 21. A. J. Krause, *et al.*, Stepwise oxygenation of the Paleozoic atmosphere. *Nat. Commun.* **9**, 1–10  
569 (2018).
- 570 22. T. M. Lenton, S. J. Daines, B. J. W. Mills, COPSE reloaded: An improved model of  
571 biogeochemical cycling over Phanerozoic time. *Earth-Science Rev.* **178**, 1–28 (2018).
- 572 23. R. Tostevin, B. J. W. W. Mills, Reconciling proxy records and models of Earth’s oxygenation  
573 during the Neoproterozoic and Palaeozoic. *Interface Focus* (2020)  
574 <https://doi.org/10.1098/rsfs.2019.0137>.
- 575 24. E. A. Sperling, C. A. Frieder, L. A. Levin, Biodiversity response to natural gradients of multiple  
576 stressors on continental margins. *Proc. R. Soc. B Biol. Sci.* **283** (2016).
- 577 25. E. Sampaio, *et al.*, Impacts of hypoxic events surpass those of future ocean warming and  
578 acidification. *Nat. Ecol. Evol.* (2021) <https://doi.org/10.1038/s41559-020-01370-3>.
- 579 26. L. A. Levin, “Oxygen Minimum Zone Benthos: Adaptation and Community Response to Hypoxia”

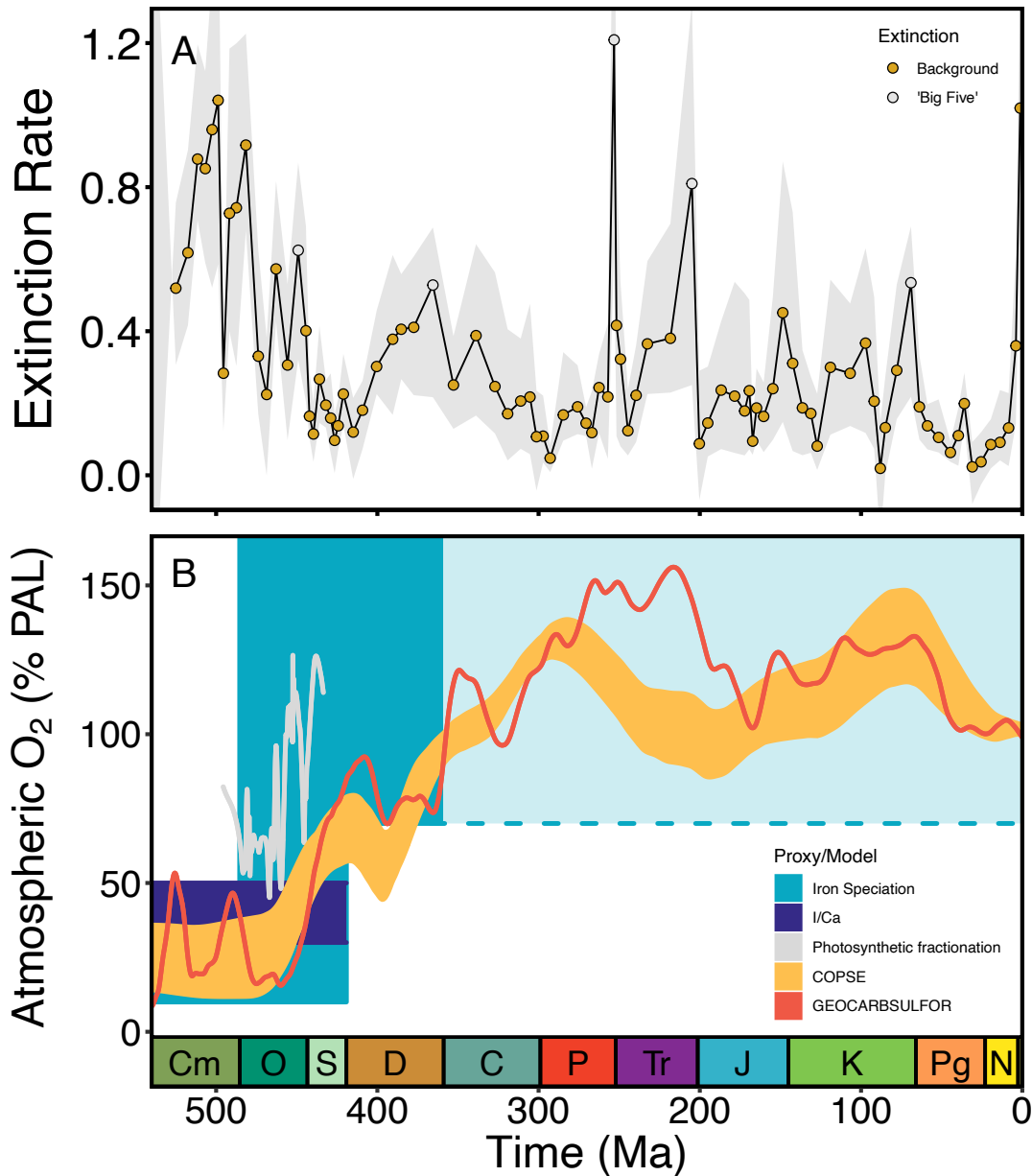
- 580 in *Oceanography and Marine Biology, An Annual Review, Volume 41*, (CRC Press, 2003), pp. 1–  
581 45.
- 582 27. H. O. Pörtner, A. P. Farrell, Physiology and climate change. *Science* **322**, 690–692 (2008).  
583 28. H. O. Pörtner, Oxygen- And capacity-limitation of thermal tolerance: A matrix for integrating  
584 climate-related stressor effects in marine ecosystems. *J. Exp. Biol.* **213**, 881–893 (2010).  
585 29. C. Deutsch, A. Ferrel, B. Seibel, H. O. Pörtner, R. B. Huey, Climate change tightens a metabolic  
586 constraint on marine habitats. *Science* **348**, 1132–1135 (2015).  
587 30. E. M. Howard, *et al.*, Climate-driven aerobic habitat loss in the California Current System. *Sci.*  
588 *Adv.* **6**, eaay3188 (2020).  
589 31. M. I. Duncan, N. C. James, W. M. Potts, A. E. Bates, Different drivers, common mechanism; the  
590 distribution of a reef fish is restricted by local-scale oxygen and temperature constraints on aerobic  
591 metabolism. *Conserv. Physiol.* **8** (2020).  
592 32. T. H. Boag, W. Gearty, R. G. Stockey, Metabolic tradeoffs control biodiversity gradients through  
593 geological time. *Curr. Biol.* (2021) <https://doi.org/10.1016/j.cub.2021.04.021>.  
594 33. J. L. Penn, C. Deutsch, J. L. Payne, E. A. Sperling, Temperature-dependent hypoxia explains  
595 biogeography and severity of end-Permian marine mass extinction. *Science* **362**, eaat1327 (2018).  
596 34. C. J. Reddin, P. S. Nätscher, Á. T. Kocsis, H. O. Pörtner, W. Kiessling, Marine clade sensitivities to  
597 climate change conform across timescales. *Nat. Clim. Chang.* **10**, 249–253 (2020).  
598 35. T. H. Boag, R. G. Stockey, L. E. Elder, P. M. Hull, E. A. Sperling, Oxygen, temperature and the  
599 deep-marine stenothermal cradle of Ediacaran evolution. *Proc. R. Soc. B Biol. Sci.* **285**, 20181724  
600 (2018).  
601 36. C. T. Reinhard, N. J. Planavsky, S. L. Olson, T. W. Lyons, D. H. Erwin, Earth’s oxygen cycle and  
602 the evolution of animal life. *Proc. Natl. Acad. Sci.* **113**, 8933–8938 (2016).  
603 37. E. A. Sperling, A. H. Knoll, P. R. Girguis, The Ecological Physiology of Earth’s Second Oxygen  
604 Revolution. *Annu. Rev. Ecol. Evol. Syst.* **46**, 215–235 (2015).  
605 38. C. Deutsch, J. L. Penn, B. Seibel, Metabolic trait diversity shapes marine biogeography. *Nature*  
606 **585**, 557–562 (2020).  
607 39. A. Ridgwell, *et al.*, Marine geochemical data assimilation in an efficient Earth system model of  
608 global biogeochemical cycling. *Biogeosciences* **4**, 87–104 (2007).  
609 40. C. J. Reddin, Á. T. Kocsis, W. Kiessling, Climate change and the latitudinal selectivity of ancient  
610 marine extinctions. *Paleobiology* **45**, 70–84 (2019).  
611 41. E. E. Saupe, *et al.*, Extinction intensity during Ordovician and Cenozoic glaciations explained by  
612 cooling and palaeogeography. *Nat. Geosci.* **13**, 65–70 (2020).  
613 42. K. M. Meyer, A. Ridgwell, J. L. Payne, The influence of the biological pump on ocean chemistry:  
614 implications for long-term trends in marine redox chemistry, the global carbon cycle, and marine  
615 animal ecosystems. *Geobiology* **14**, 207–219 (2016).  
616 43. M. Gutjahr, *et al.*, Very large release of mostly volcanic carbon during the Palaeocene-Eocene  
617 Thermal Maximum. *Nature* **548**, 573–577 (2017).  
618 44. G. L. Foster, D. L. Royer, D. J. Lunt, Future climate forcing potentially without precedent in the  
619 last 420 million years. *Nat. Commun.* **8** (2017).  
620 45. S. N. C. Woolley, *et al.*, Deep-sea diversity patterns are shaped by energy availability. *Nature* **533**,  
621 393–396 (2016).  
622 46. E. A. Sperling, R. G. Stockey, The temporal and environmental context of early animal evolution:  
623 Considering all the ingredients of an “explosion.” *Integr. Comp. Biol.* **58**, 605–622 (2018).  
624 47. B. A. Seibel, C. Deutsch, Oxygen supply capacity in animals evolves to meet maximum demand at  
625 the current oxygen partial pressure regardless of size or temperature. *J. Exp. Biol.* **223**, jeb.210492  
626 (2020).  
627 48. T. W. Hearing, *et al.*, An early Cambrian greenhouse climate. *Sci. Adv.* **4**, eaar5690 (2018).  
628 49. J. A. Trotter, I. S. Williams, C. R. Barnes, C. Lecuyer, R. S. Nicoll, Did Cooling Oceans Trigger  
629 Ordovician Biodiversification? Evidence from Conodont Thermometry. *Science* **321**, 550–554  
630 (2008).  
631 50. S. L. Goldberg, T. M. Present, S. Finnegan, K. D. Bergmann, A high-resolution record of early  
632 Paleozoic climate. *Proc. Natl. Acad. Sci.* **118**, e2013083118 (2021).  
633 51. C. Vérard, J. Veizer, On plate tectonics and ocean temperatures. *Geology* **47**, 882–885 (2019).

- 634 52. B. J. W. Mills, *et al.*, Modelling the long-term carbon cycle, atmospheric CO<sub>2</sub>, and Earth surface  
635 temperature from late Neoproterozoic to present day. *Gondwana Res.* **67**, 172–186 (2019).
- 636 53. K. D. Bergmann, *et al.*, A paired apatite and calcite clumped isotope thermometry approach to  
637 estimating Cambro-Ordovician seawater temperatures and isotopic composition. *Geochim.*  
638 *Cosmochim. Acta* **224**, 18–41 (2018).
- 639 54. R. A. Close, R. B. J. Benson, E. E. Saupe, M. E. Clapham, R. J. Butler, The spatial structure of  
640 Phanerozoic marine animal diversity. *Science* **368**, 420–424 (2020).
- 641 55. A. R. Palmer, Trilobites of the Late Cambrian pterocephaliid biomere in the Great Basin, United  
642 States. *U. S. Geol. Surv. Prof. Pap.* **493**, 1–104 (1965).
- 643 56. A. R. Palmer, The biomere problem: evolution of an idea. *J. Paleontol.* **58**, 599–611 (1984).
- 644 57. R. A. Fortey, There are Extinctions and Extinctions: Examples from the Lower Palaeozoic. *Philos.*  
645 *Trans. R. Soc. B Biol. Sci.* **325**, 327–355 (1989).
- 646 58. M. R. Saltzman, C. T. Edwards, J. M. Adrain, S. R. Westrop, Persistent oceanic anoxia and  
647 elevated extinction rates separate the Cambrian and Ordovician radiations. *Geology* **43**, 807–810  
648 (2015).
- 649 59. B. C. Gill, *et al.*, Geochemical evidence for widespread euxinia in the Later Cambrian ocean.  
650 *Nature* **469**, 80–83 (2011).
- 651 60. M. Elrick, S. Rieboldt, M. Saltzman, R. M. McKay, Oxygen-isotope trends and seawater  
652 temperature changes across the Late Cambrian Steptoean positive carbon-isotope excursion (SPICE  
653 event). *Geology* **39**, 987–990 (2011).
- 654 61. M. A. LeRoy, B. C. Gill, E. A. Sperling, N. R. McKenzie, T.-Y. S. Park, Variable redox conditions  
655 as an evolutionary driver? A multi-basin comparison of redox in the middle and later Cambrian  
656 oceans (Drumian-Paibian). *Palaeogeogr. Palaeoclimatol. Palaeoecol.*, 110209 (2021).
- 657 62. A. Y. Zhuravlev, R. A. Wood, Anoxia as the cause of the mid-Early Cambrian (Botomian)  
658 extinction event. *Geology* **24**, 311–314 (1996).
- 659 63. W. Yao, A. Paytan, U. G. Wortmann, Large-scale ocean deoxygenation during the Paleocene-  
660 Eocene thermal maximum. *Science* **361**, 804–806 (2018).
- 661 64. H. C. Jenkyns, Geochemistry of oceanic anoxic events. *Geochemistry, Geophys. Geosystems* **11**  
662 (2010).
- 663 65. M. O. Clarkson, *et al.*, Uranium isotope evidence for two episodes of deoxygenation during  
664 Oceanic Anoxic Event 2. *Proc. Natl. Acad. Sci.* **115**, 201715278 (2018).
- 665 66. D. H. Erwin, Lessons from the past: Biotic recoveries from mass extinctions. *Proc. Natl. Acad. Sci.*  
666 *U. S. A.* **98**, 5399–5403 (2001).
- 667 67. A. H. Knoll, Systems paleobiology. *Bull. Geol. Soc. Am.* **125**, 3–13 (2013).
- 668 68. A. H. Knoll, R. K. Bambach, J. L. Payne, S. Pruss, W. W. Fischer, Paleophysiology and end-  
669 Permian mass extinction. *Earth Planet. Sci. Lett.* **256**, 295–313 (2007).
- 670 69. J. L. Payne, M. E. Clapham, End-permian mass extinction in the oceans: An ancient analog for the  
671 twenty-first century? *Annu. Rev. Earth Planet. Sci.* **40**, 89–111 (2012).
- 672 70. J. X. Fan, *et al.*, A high-resolution summary of Cambrian to early Triassic marine invertebrate  
673 biodiversity. *Science* **367**, 272–277 (2020).
- 674 71. A. Mehra, *et al.*, Curation and Analysis of Global Sedimentary Geochemical Data to Inform Earth  
675 History. *GSA Today* **31**, 4–9 (2021).
- 676 72. Ú. C. Farrell, *et al.*, The Sedimentary Geochemistry and Paleoenvironments Project. *Geobiology*,  
677 gbi.12462 (2021).
- 678 73. K. W. Flessa, D. Jablonski, Declining Phanerozoic background extinction rates: Effect of  
679 taxonomic structure? *Nature* **313**, 216–218 (1985).
- 680 74. K. M. Meyer, L. R. Kump, A. Ridgwell, Biogeochemical controls on photic-zone euxinia during  
681 the end-Permian mass extinction. *Geology* **36**, 747–750 (2008).
- 682 75. A. Pohl, *et al.*, Glacial onset predated Late Ordovician climate cooling. *Paleoceanography* **31**, 800–  
683 821 (2016).
- 684 76. D. O. Gough, “Solar Interior Structure and Luminosity Variations” in *Physics of Solar Variations*,  
685 (Springer Netherlands, 1981), pp. 21–34.
- 686 77. A. F. Hofmann, E. T. Peltzer, P. M. Walz, P. G. Brewer, Hypoxia by degrees: Establishing  
687 definitions for a changing ocean. *Deep. Res. Part I Oceanogr. Res. Pap.* **58**, 1212–1226 (2011).

- 688 78. C. T. Edwards, M. R. Saltzman, D. L. Royer, D. A. Fike, Oxygenation as a driver of the Great  
689 Ordovician Biodiversification Event. *Nat. Geosci.* **10**, 925–929 (2017).  
690  
691

692 **Figures**

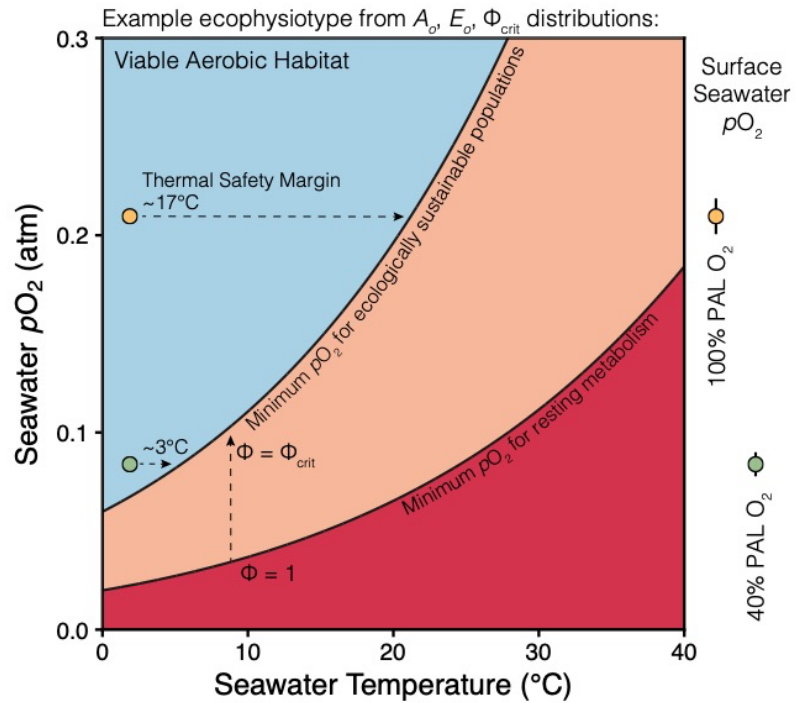
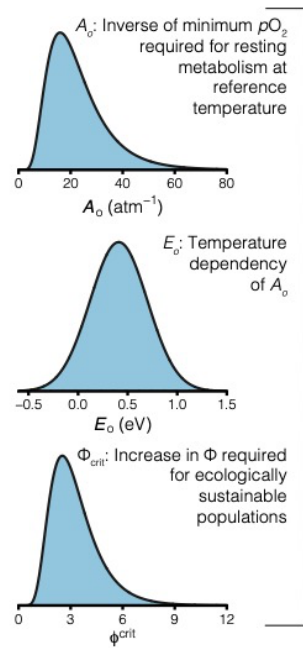
693



694  
 695 Figure 1: Trends in atmospheric oxygen and extinction rates through the Phanerozoic. A) Genus-level  
 696 extinction rates for marine ectotherms (adapted from Kocsis et al. (7), *Materials and Methods*) – line  
 697 and points represent mean values, envelope represents maximum and minimum estimates from all 12  
 698 methodological approaches (3 treatments: raw, classical rarefaction and Shareholder Quorum  
 699 Subsampling-standardized, for each of 4 metrics: average per capita rates, corrected three-timer rates,  
 700 gap-filler rates and second-for-third substitution rates). B) Reconstructions of atmospheric oxygen  
 701 from biogeochemical models (21, 22, 78) and geochemical proxy records (15, 17).

702

Metabolic Index parameters:

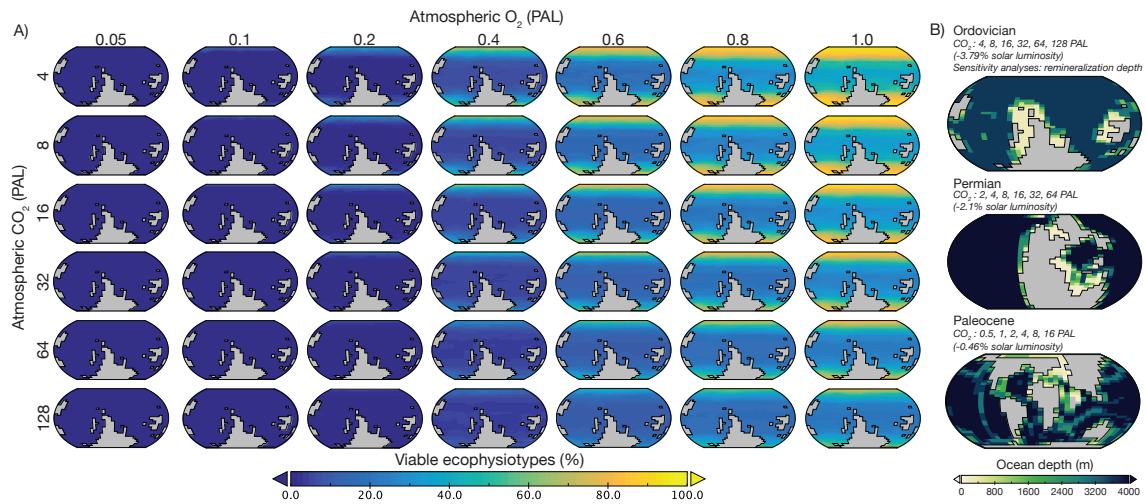


703

704

Figure 2: Schematic of ecophysiological model based on the Metabolic Index (Equation 1). The frequency distributions of three key ecophysiological parameters –  $A_o$ ,  $E_o$  and  $\Phi_{crit}$  – are illustrated to the left. The implications of these parameters for the ecophysiological modeling framework employed in this study are illustrated for an example ecophysiotype on the right, based on the median values of these distributions. The minimum seawater  $pO_2$  required for resting metabolism increases at an exponential rate, primarily due to temperature effects on metabolic rate. The minimum seawater  $pO_2$  required for sustainable populations on ecological timescales also increases exponentially with temperature (faster than the minimum  $pO_2$  required for resting metabolism), as the product of an exponential function defined by  $A_o$ ,  $E_o$  and  $\Phi_{crit}$  (see *Materials and Methods*, Equation 1 for full details). At a given temperature, the thermal safety margin of a hypothetical ecophysiotype is predicted to decrease with decreasing seawater  $pO_2$  (either due to a change in equilibrium oxygen levels resulting from decreasing atmospheric oxygen, or a decrease in saturation resulting from biogeochemical processes such as organic carbon remineralization). Surface seawater  $pO_2$  distributions (far right) are taken from Earth system model analyses presented in this study (8 PAL CO<sub>2</sub> Ordovician configuration; points represent mean values, and error bars 2 SD).

719

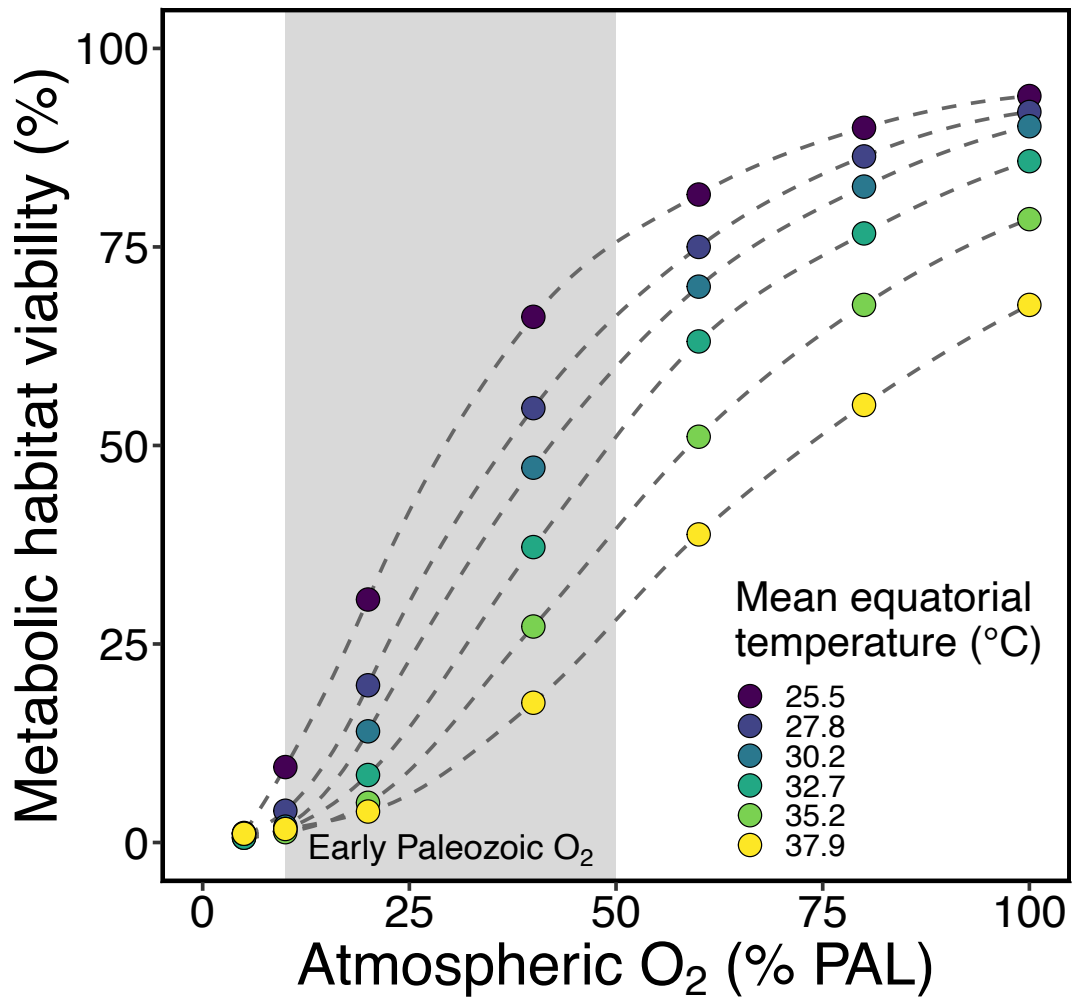


720

721 Figure 3: Ensemble Earth system modeling approach using cGENIE. A) Example of ensemble O<sub>2</sub>-CO<sub>2</sub>  
 722 Earth system modeling experiment using Ordovician continental configuration with modern  
 723 remineralization depth. Color scale illustrates the proportion of the modeled ecophysiotypes that can  
 724 live in each cell of the surface ocean (top 0-80m layer of the 16 layer cGENIE ocean is illustrated  
 725 here). B) Sensitivity analyses performed in this study. Variations in continental configuration,  
 726 remineralization depth and CO<sub>2</sub> forcing are detailed here. The atmospheric O<sub>2</sub> levels investigated in  
 727 each ensemble experiment are the same. We present full surface ocean models here for ease of visual  
 728 comparison, although main text analyses use only non-polar shelf environments (as illustrated in Fig.  
 729 S3).

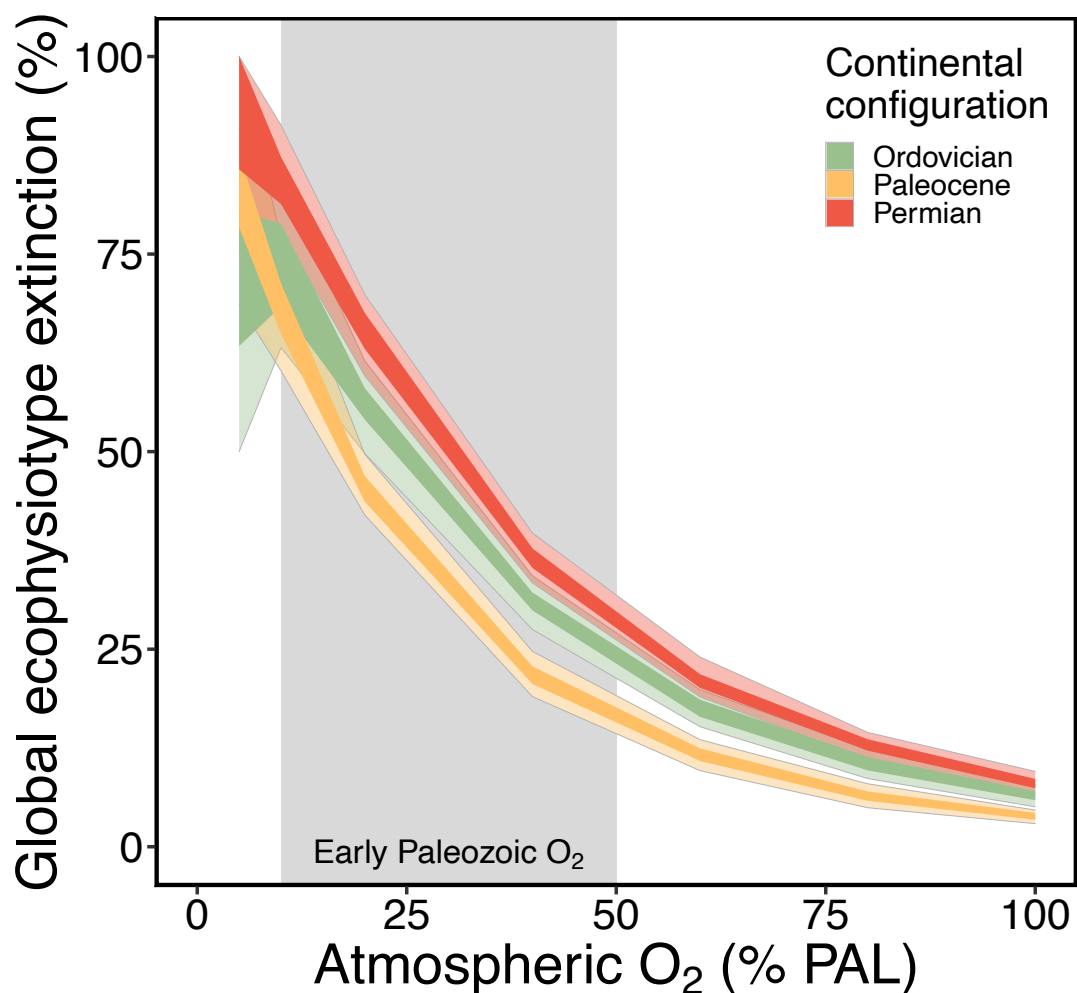
730

731



732  
 733 Figure 4: Metabolic habitat viability for the ensemble O<sub>2</sub>-CO<sub>2</sub> Earth system modeling experiment with  
 734 an Ordovician continental configuration and modern remineralization depth. Metabolic habitat  
 735 viability is calculated as the proportion of the ecophysiotypes modeled that can live in shelf  
 736 environments of each three dimensional ocean model produced using cGENIE (*Materials and*  
 737 *Methods*). Circles represent individual experiments and are color coded by mean equatorial sea surface  
 738 temperature (-3.2°S to 3.2°N, 0-80m depth), as a product of atmospheric CO<sub>2</sub> forcing.

739



740  
 741 Figure 5: Global ecophysiotype extinction predicted to result from a ~5°C warming event from an  
 742 approximately pre-industrial baseline sea surface temperature at different atmospheric O<sub>2</sub> levels,  
 743 illustrating sensitivity analyses evaluating the influence of continental configuration on predicted  
 744 extinction. Global ecophysiotype extinction is defined as the proportion of ecophysiotypes that were  
 745 viable in the shelf environments of the colder baseline simulation but are no longer viable in any cell  
 746 of the shelf environments of the warmer ocean simulation (*Materials and Methods*). Baseline CO<sub>2</sub>  
 747 levels used: 1 PAL – Paleocene; 8 PAL – Permian; 8 PAL – Ordovician. Darker envelopes represent  
 748 25<sup>th</sup>-75<sup>th</sup> percentiles of 100 simulation results, lighter envelopes represent 5<sup>th</sup>-95<sup>th</sup> percentiles.